

# Commensurate growth and diminishing substrate influence in a multilayer film of a tris(thieno)hexaazatriphenylene derivative on Au(111) studied by scanning tunneling microscopy

Sieu D. Ha,<sup>1,\*</sup> Qing Zhang,<sup>2</sup> Stephen Barlow,<sup>2</sup> Seth R. Marder,<sup>2</sup> and Antoine Kahn<sup>1</sup>

<sup>1</sup>*Department of Electrical Engineering, Princeton University, Princeton, New Jersey 08544, USA*

<sup>2</sup>*School of Chemistry and Biochemistry and Center for Organic Photonics and Electronics, Georgia Institute of Technology, Atlanta, Georgia 30332, USA*

(Received 10 October 2007; published 28 February 2008)

Layer-by-layer growth of the electron-transport material tris{2,5-bis(3,5-bis-trifluoromethyl-phenyl)-thieno}[3,4-*b,h,n*]-1,4,5,8,9,12-hexaazatriphenylene (THAP) on Au(111) is probed by scanning tunneling microscopy (STM). A relative of discotic liquid crystalline molecules, THAP is shown to grow in commensurate ordered planes from the first to fourth monolayers. The four monolayers all show a concordant ordered structure in which the molecules arrange parallel to the substrate in a hexagonal close-packed lattice with a herringbone pattern defined by alternating rows of molecules with antiparallel orientation. The unit cell is rectangular with two molecules per cell and is nearly equivalent for each layer. The spatial broadening of the local density of states due to the metallic substrate is appreciably diminished in upper layers, as expected and as evidenced by the localization of states seen in STM. There is good agreement between the highest occupied molecular orbital obtained in density functional theory calculations for a single molecule and STM images of the upper layers, in accord with the localized nature of electronic states on molecules under minimal substrate influence.

DOI: [10.1103/PhysRevB.77.085433](https://doi.org/10.1103/PhysRevB.77.085433)

PACS number(s): 68.37.Ef

## I. INTRODUCTION

Of key importance to realize commercially viable organic electronic devices is the development of electron-transport materials (ETMs) of comparable performance to current hole-transport materials such as pentacene<sup>1</sup> and rubrene.<sup>2</sup> Such materials are necessary to fabricate, among others, organic light emitting diodes and electron-channel field effect transistors, devices critical for consumer electronics. Among molecular compounds currently under development are derivatives of the discoid molecule hexaazatriphenylene (HATNA),<sup>3,4</sup> some of which have mobilities as high as 0.3 cm<sup>2</sup>/V s in their columnar discotic liquid crystalline (LC) phase.<sup>5</sup> Discoid molecules often stack into columnar structures which promote  $\pi$ - $\pi$  overlapping between adjacent molecules and thus expedite electron hopping along the columns. HATNA derivatives and analogs are also attractive as ETMs because they have relatively high electron affinities (EAs), which facilitate electron injection from commonly used metallic contacts and also widen the possibilities for n-type doping of films.<sup>6</sup>

One such HATNA analog with high EA is tris{2,5-bis(3,5-bis-trifluoromethyl-phenyl)-thieno}[3,4-*b,h,n*]-1,4,5,8,9,12-hexaazatriphenylene (THAP), the chemical structure of which is illustrated in Fig. 1(a) (inset). Density functional theory (DFT) calculations demonstrate that the thiophene and bis(trifluoromethyl)phenyl groups contribute significantly to make the molecule more electronegative than HATNA by 1.74 eV.<sup>6</sup> This was successfully exploited in studies wherein the organometallic complex cobaltocene was reported to n-type dope THAP.<sup>7,8</sup> In addition, the fluorine groups may also enhance the stability of THAP devices in air, as with fluorinated naphthalenetetracarboxylic diimide<sup>9</sup> and copper phthalocyanine.<sup>10</sup> As THAP displays promise as a viable ETM, it is necessary and interesting to determine how it grows and orders on a metal substrate.

Interfacial molecular order has been investigated with scanning tunneling microscopy (STM) on triphenylene<sup>11-14</sup> and hexaazatriphenylene<sup>15</sup> derivatives, as well as HATNA,<sup>16</sup> but no studies have sufficiently explored ordered growth beyond the first monolayer. Moreover, the bulk crystal structure of THAP is unknown. In this paper, STM results illustrate ordered growth of THAP on Au(111) from the first to fourth monolayers. The structure of the first to fourth monolayers is equivalent, which suggests that thick films of THAP could be highly ordered, an advantageous characteristic for efficient carrier transport.

## II. EXPERIMENTAL METHODS

Au(111)/mica substrates annealed by hydrogen flame were purchased from Molecular Imaging. After loading into ultrahigh vacuum (UHV), the substrates were cleaned by repeated cycles of Ar<sup>+</sup> sputtering (0.5 kV) and annealing (710 K), which produced clean surfaces with terraces typically about 100–200 nm wide, exhibiting the standard  $22 \times \sqrt{3}$  reconstruction of Au(111) as observed by STM. THAP was synthesized and purified as described previously.<sup>6</sup> THAP molecules were deposited in monolayer intervals onto Au(111)/mica by thermal evaporation from a quartz crucible in UHV ( $1.0 \times 10^{-10}$  Torr) at about 0.5 Å/min (480 K), with the substrate at room temperature. Thickness was calibrated by referencing a quartz crystal microbalance and comparing with images of the first monolayer in STM. Unless specified in the discussion, no post-deposition annealing was necessary to obtain ordered films.

Samples were analyzed in an interconnected UHV chamber ( $4.0 \times 10^{-11}$  Torr) equipped with a room-temperature Omicron scanning tunneling microscope. All images were taken in constant-current mode, in which the tip-sample separation varies to maintain constant tunneling current at

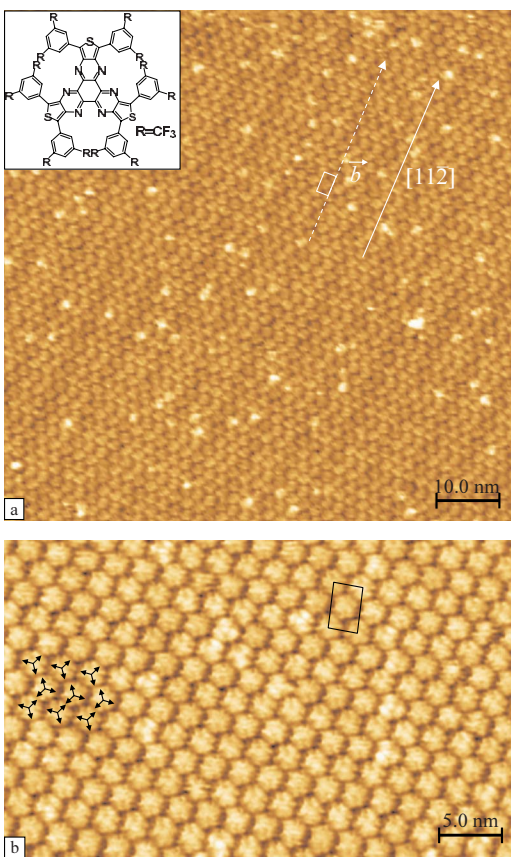


FIG. 1. (Color online) STM images of (a) 1 ML THAP/Au(111) with arrows illustrating alignment between unit cell vector  $\vec{b}$  and  $[11\bar{2}]$  direction of substrate ( $80.0 \times 80.0 \text{ nm}^2$ ,  $V_{\text{sample}} = -1.5 \text{ V}$ , and  $I = 100 \text{ pA}$ ) (inset: chemical structure of THAP) and (b) small area view showing antiparallel molecular orientation [unit cell illustrated ( $40.0 \times 25.0 \text{ nm}^2$ ,  $V_{\text{sample}} = -1.5 \text{ V}$ , and  $I = 80 \text{ pA}$ )].

fixed bias. Tungsten STM tips were electrochemically etched from 0.25 mm wire in 2 M NaOH solution using a tip-etch circuit.<sup>17</sup> They were loaded into UHV and electron-bombarded *in situ* to remove the native oxide. STM images were processed with WSXM software from Nanotec Electronica, Spain.<sup>18</sup>

### III. RESULTS AND DISCUSSION

#### A. First monolayer

THAP molecules deposited on the crystalline surface of Au(111) readily diffuse at room temperature and form an ordered monolayer, as seen in Fig. 1(a). The adlayer is characterized by a herringbone-type hexagonal close-packed (hcp) structure in which molecules in alternate rows adopt antiparallel orientations, modulo a  $120^\circ$  rotation due to the threefold symmetry of the molecules. This is more clearly illustrated by the rows of trigonal shapes in Fig. 1(b), which is a smaller area scan of the first monolayer. The order is not unusual as other derivatives of triphenylene also display a similar alternating configuration.<sup>11,14,19</sup> The herringbone may be due to steric hindrance between nearest neighbor aromatic cores which promotes an antiparallel configuration,<sup>12,15</sup> al-

though detailed calculations would be needed to confirm this statement. In a standard hcp film, the unit cell would be rhomboidal; however, due to the herringbone arrangement of THAP/Au(111), the unit cell of the first monolayer is rectangular. The dimensions of the unit cell are  $a = 21.8 \pm 0.2 \text{ \AA}$ ,  $b = 32.5 \pm 0.1 \text{ \AA}$ , and  $\Gamma = 88.7 \pm 0.6^\circ$ , with two molecules per cell.

The molecules in Fig. 1(b) correspond well with the chemical model inset in Fig. 1(a). They are approximately hexagonal in shape and also show submolecular features that can be attributed to the phenyl substituents. Upon closer inspection, the molecules appear to be threefold symmetric, as expected. The molecular dimensions (approximate disks with average diameter of  $\sim 21 \text{ \AA}$ ) are in good agreement with DFT calculations,<sup>6</sup> indicating that the molecules lie flat on the Au(111) surface. Note that despite the high-resolution features, the molecules are generally uniform in color. This implies that the local density of states (LDOS) has minimal variation in the first monolayer of THAP adsorbed on Au(111). In Fig. 1, the sample bias voltage is negative with respect to the tip, thus the highest occupied molecular orbital (HOMO) is the principal energy level in tunneling.<sup>20</sup> However, calculations of the HOMO distribution on a single THAP molecule show a more discrete submolecular structure in which the density of states is localized around the three thiophene rings [Fig. 4(b), inset].<sup>6</sup> The difference in appearance between the HOMO and the molecules in first monolayer STM images suggests that the metallic substrate must influence the electronic properties of the organic layer and cause spatial broadening of states.

The image in Fig. 1(a) has scattered bright features that are likely adsorbed defects or excess molecules of the partially formed second monolayer. The figure also shows traces of the underlying Au(111) reconstruction pattern, which is an effect of the bare metallic surface manifested in STM by alternating rows of bright and dark contrasts.<sup>21</sup> Visibility of the reconstruction indicates that the electron tail of the substrate is not fully suppressed by adsorption of 1 ML THAP. The bright rows are soliton walls, which run in the  $[11\bar{2}]$  direction and are caused by alternating regions of abutting face-centered cubic and hcp structures.<sup>22</sup> Most surfaces of Au(111) also have a second-order reconstruction in which the soliton walls zigzag at  $120^\circ$  angles with  $\sim 250 \text{ \AA}$  period. This does not appear in Fig. 1(a), but is evident in the lower part of Fig. 2(b), which is a low-pass filtered STM image of 1 ML THAP/Au(111). Moreover, there are three rotationally equivalent domains of Au(111) and terraces with zigzag features contain two of the domains, one each on the “zig” and the “zag” regions. Terraces without the secondary reconstruction contain only one domain.

The appearance of the Au(111) reconstruction in STM images of organic molecules can be used to determine the relationship between the adlayer and substrate orientations. In the case of 1 ML THAP, the long unit cell vector  $\vec{b}$  generally aligns with the  $[11\bar{2}]$  direction of the substrate to within  $\sim 2^\circ$ , as illustrated in Fig. 1(a). Thus, the metallic substrate affects the arrangement of THAP domains. This is further demonstrated in Fig. 2(a), which shows two equivalent domains of THAP adsorbed on a single Au(111) terrace.

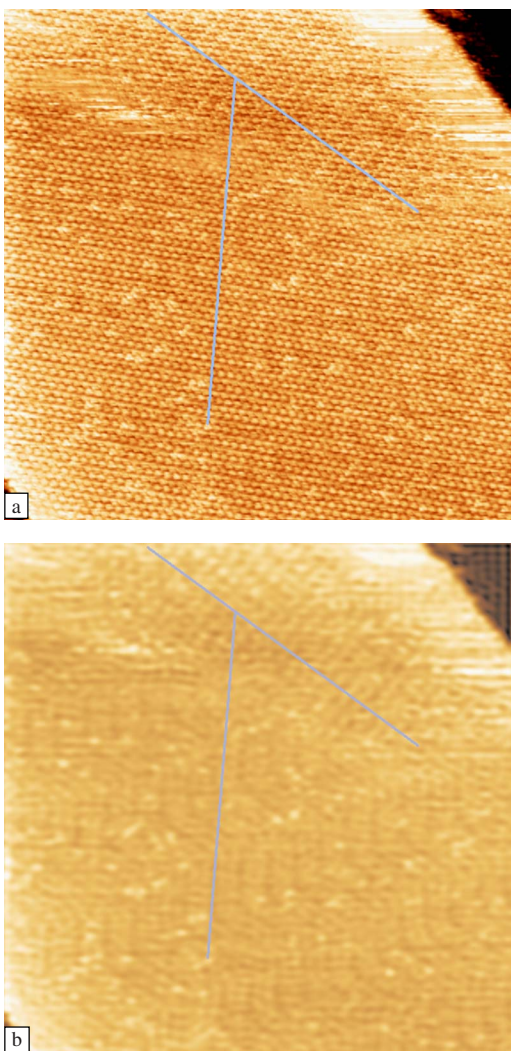


FIG. 2. (Color online) STM images of (a) 1 ML THAP/Au(111) ( $125.3 \times 125.3 \text{ nm}^2$ ,  $V_{\text{sample}} = -1.5 \text{ V}$ , and  $I = 80 \text{ pA}$ ) and (b) low-pass filtered version demonstrating simultaneous alignment of two molecular domains with two rotationally equivalent substrate domains.

The filtered version of Fig. 2(a) in Fig. 2(b) is used to accent the zigzag pattern of the substrate. The lines drawn in both figures are extensions of the unit cell vector  $\vec{b}$  of each molecular domain, and it is clear that each is parallel to one of two orientations of the soliton walls. Indeed, each domain of THAP is equivalent by a rotation of approximately  $121^\circ$ , in good agreement with the rotational equivalence of the substrate domains. Although the molecules tend to align with the substrate, the THAP-Au(111) interface can be qualified as a weak van der Waals interaction since the periodicity of the Au(111) reconstruction is undisturbed upon THAP adsorption. This is similar to the case of 3,4,9,10-perylenetetracarboxylic dianhydride/Au(111) (Ref. 23) and is in contrast to hexabenzocoronene,<sup>24</sup> which has a strong interaction with Au(111) and modifies the substrate reconstruction. In correlation with the weak interaction, there exist a few instances of dual molecular domains on a single terrace without strong substrate registry (not shown). The unit cell

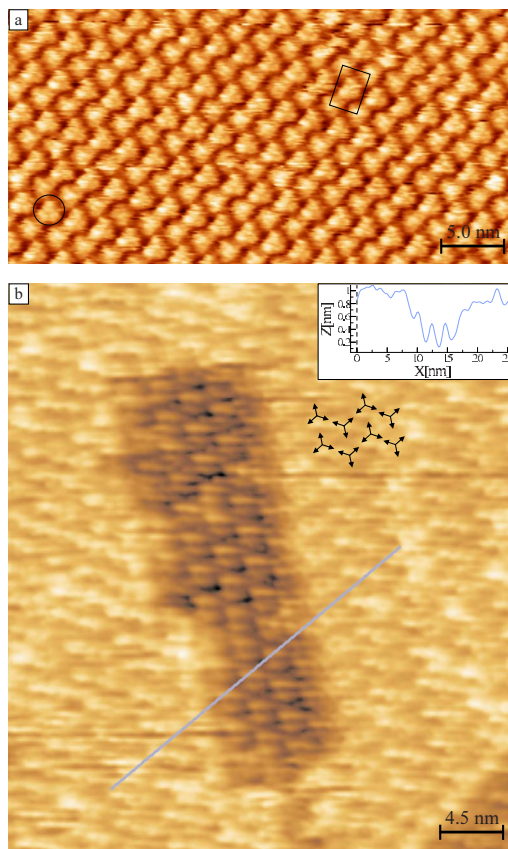


FIG. 3. (Color online) STM images of (a) 2 ML THAP/Au(111) in same herringbone hcp ordering as first monolayer [unit cell illustrated ( $40.0 \times 20.0 \text{ nm}^2$ ,  $V_{\text{sample}} = +1.8 \text{ V}$ , and  $I = 80 \text{ pA}$ )] and (b) partial 2 ML THAP/Au(111) showing commensurate growth between the first two monolayers ( $36.0 \times 40.0 \text{ nm}^2$ ,  $V_{\text{sample}} = -2.0 \text{ V}$ , and  $I = 80 \text{ pA}$ ). Inset: height profile illustrating  $\sim 4 \text{ \AA}$  apparent step size between first and second monolayers.

vectors of each domain are still rotated with respect to each other by about  $120^\circ$ , but the alignment with the substrate is off by about  $17^\circ$ . There may be some competition between molecular domains to control the orientation, in which case the molecule-molecule interaction may override the weak molecule-substrate interaction and disorient the organic layer with respect to the substrate.

## B. Second monolayer

The second monolayer of THAP deposited on Au(111) displays the same order as the first monolayer, namely, an hcp structure with alternating rows of molecular orientation. As seen in Fig. 3(a), the unit cell is again rectangular with two molecules per cell, and the dimensions are similar to the first monolayer, with  $a = 20.9 \pm 0.1 \text{ \AA}$ ,  $b = 35.2 \pm 0.1 \text{ \AA}$ , and  $\Gamma = 89.4 \pm 0.2^\circ$ . Though the image here is not as well resolved as in Fig. 1(b), the alternating orientation between rows is more obvious. The soliton walls of the Au(111) reconstruction are no longer visible in STM images of the second monolayer, indicating that the spatial extent of substrate electronic states does not extend farther than two monolayers of THAP. There is therefore correspondingly less

substrate influence and smearing of the overlayer LDOS. Indeed, certain molecules in Fig. 3(a), one of which is circled, are not uniform in color and show some discrete submolecular features. This effect is discussed in greater depth in the next section.

As the second monolayer of THAP deposited on Au(111) orders in the same manner and with similar unit cell dimensions as the first monolayer, the growth is expected to be commensurate. Figure 3(b) shows an STM image of an incomplete second monolayer in which both monolayers are probed simultaneously. Inset in the figure is a height profile along the illustrated line showing an apparent step size of about 4 Å between the first and second monolayers. While the bulk crystal structure of THAP is unknown, the measured height is slightly larger than interplanar distances of HATNA derivatives,<sup>6</sup> which is expected due to the out-of-plane twist of the bis(trifluoromethyl)phenyl groups. It is apparent from the image that the rows of molecules in both layers are parallel in all three directions and that the intermolecular distances are nearly equal. This is strong evidence for commensurate growth. However, in this image, it appears as though the orders of the two layers do not agree. Despite the poor resolution, the second monolayer in Fig. 3(b) is ordered in the familiar herringbone hcp structure, as demonstrated by the trigonal shapes. Yet in the figure, the first monolayer appears to be in an hcp configuration without discernable alternation of molecular orientation. This may simply be an electronic effect whereby adsorption of an additional THAP layer broadens the states of the first layer such that molecular orientation is no longer observable, although it may still be present. Alternatively, it may be a physical effect in which the second monolayer modifies the structure of the first monolayer such that all molecules are oriented in the same direction or all are rotationally disordered. The latter scenario would suggest that Au(111) does not anchor the order of the first monolayer, but rather interlayer and intralayer molecule-molecule forces primarily control the configuration of the entire THAP film. Whichever the explanation for the noted difference in apparent order, it is clear that, disregarding molecular orientation, the second monolayer is commensurate with the first.

### C. Third monolayer

STM topographs of two distinct phases of the third monolayer of THAP/Au(111) are shown in Fig. 4. Images of the third monolayer were recorded after lightly ramping the sample temperature to 350 K over 20 min and allowing it to cool back to room temperature. This was intended to desorb excess molecules, which interfere with the tip during microscopy, at a sufficiently low temperature as to not disturb the lattice ordering. The third monolayer generally orders in the same manner as the first two monolayers, as seen in Fig. 4(a). The unit cell dimensions are slightly skewed due to sample drift, but they are still in reasonable agreement with the first two layers, with  $a=19.1 \pm 0.3$  Å,  $b=31.9 \pm 0.1$  Å,  $\Gamma=79.4 \pm 0.5^\circ$ , and two molecules per cell. In a few scattered areas of the sample, however, the molecules are ordered in hcp without the herringbone pattern, as shown in

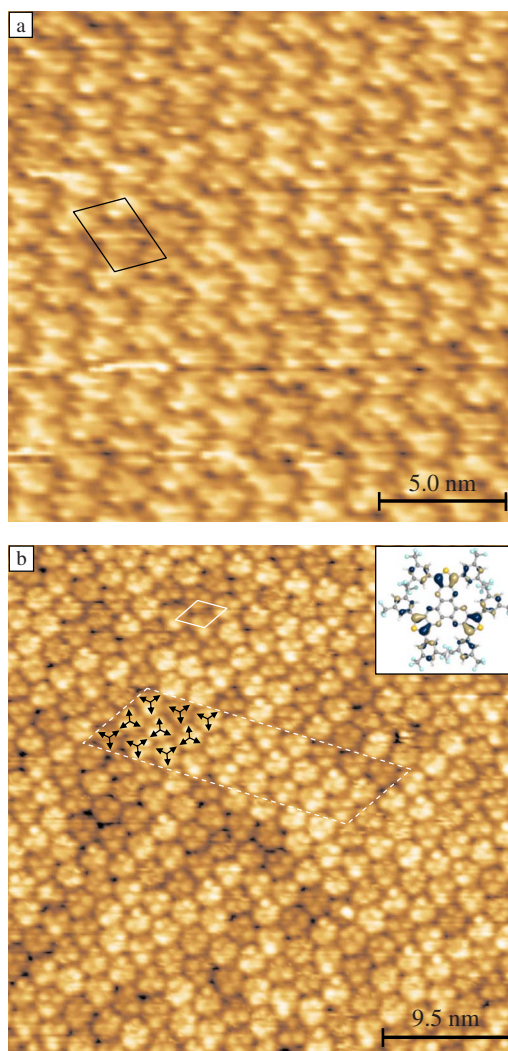


FIG. 4. (Color online) STM images of (a) 3 ML THAP/Au(111) in herringbone ordering similar to first two monolayers [unit cell illustrated ( $20.0 \times 20.0$  nm<sup>2</sup>,  $V_{\text{sample}} = -1.8$  V, and  $I = 80$  pA)] and (b) 3 ML THAP/Au(111) with rotationally disordered hcp structure [area with limited rotational order (dashed line) and unit cell (solid line) illustrated ( $38.0 \times 38.0$  nm<sup>2</sup>,  $V_{\text{sample}} = -1.8$  V, and  $I = 60$  pA)]. Inset: DFT calculation of THAP HOMO (Ref. 6).

Fig. 4(b). In this configuration, the unit cell is rhomboidal and has dimensions  $a=22.7 \pm 0.3$  Å,  $b=19.6 \pm 0.1$  Å, and  $\Gamma=54.7 \pm 0.7^\circ$  with just one molecule per cell. Some areas of the image have two to three rows with alternating orientation, as illustrated by the dashed box, but there is no long-range order of molecular orientation throughout the domain.

The existence of a disordered hexagonal phase in addition to a herringbone phase has been observed previously in triphenylene hexa-*n*-dodecanoate.<sup>25</sup> In that case, the ordered phase was characterized by molecules tilted about the columnar axis with the tilts arranged in a herringbone, while in the hexagonal phase, the tilt persisted but without correlation between columns. The transition between phases was attributed to an orientational order-disorder transition with the herringbone having a lower temperature range. In the case of THAP, the situation is presumably analogous, except considering molecular rotational orientation instead of tilt. The or-

dered herringbone phase of the third monolayer is likewise assumed to be more energetically favorable because of the same steric hindrance effects which order the second monolayer. It was also observed more often than the disordered hexagonal phase, which may have occurred at room temperature only because of substrate or film defects that propagate disorder. The STM used here is not a variable temperature system, but high and low temperature experiments would probably be able to clarify the relationship between the two phases in THAP.

There is noticeable variation in apparent height ( $\leq \sim 0.5 \text{ \AA}$ ) between molecules in Fig. 4(b). This can result from several factors. First, although THAP molecules appear flat in STM, they are not expected to be completely planar. In particular, the bis(trifluoromethyl)phenyl groups are likely to be twisted out of the plane of the core, and the tris(thieno)hexaazatriphenylene core itself may have a slightly concave or convex curvature, as seen in the crystal structure of a chlorinated HATNA.<sup>6</sup> A mixture of conformations on one substrate terrace has been observed before in STM of lead phthalocyanine on MoS<sub>2</sub>.<sup>26</sup> Second, in discotic LCs, there is typically no long-range order along a given column, i.e., the intermolecular spacing in a given column need not be fixed for all molecule pairs. This effect may propagate such that one entire column may be slightly longer than another, which is more likely for columns with few molecules and which would then be reflected in STM contrast. It is possible that THAP stacks could be similarly variant even though THAP is not liquid crystalline. Due to the relatively broad distribution of molecular heights in Fig. 4(b), defects and adsorbed excess molecules can be ruled out as causes of the height fluctuation. Such adsorbants, as seen in Figs. 1(a) and 5(a), generally only cause discrete variations in measured height.

The submolecular resolution of the third monolayer images further illustrates the diminishing substrate influence far from the interface. It is known that a metal substrate induces broadening in the energy levels of adsorbed organic molecules,<sup>27</sup> and that this effect is diminished in molecules that are farther from the interface. This is manifested in STM by the rather uniform appearance of molecules in the first two monolayers and the discrete nature of the molecular features in the third monolayer in Fig. 4(b). The image in Fig. 4(a) has comparatively poorer resolution than in Fig. 4(b) and thus it is more difficult to distinguish the features. Yet, in the latter, individual molecules appear as clusters of three small spheres arranged in an equilateral triangular shape, reflective of the threefold symmetry of the tris(thieno)hexaazatriphenylene core of THAP. Thus, the LDOS of each molecule is concentrated on three distinct areas rather than broadened throughout the molecule. As the sample bias is negative, this should correspond to the calculated spatial distribution of the single molecule HOMO of THAP. Indeed, from DFT considerations as previously discussed and as shown in the inset of Fig. 4(b), the calculated HOMO is predominantly localized in areas around each of three thiophene rings with the same symmetry as molecules in Fig. 4(b). There is therefore good agreement between STM experiments and DFT calculations for THAP/Au(111).

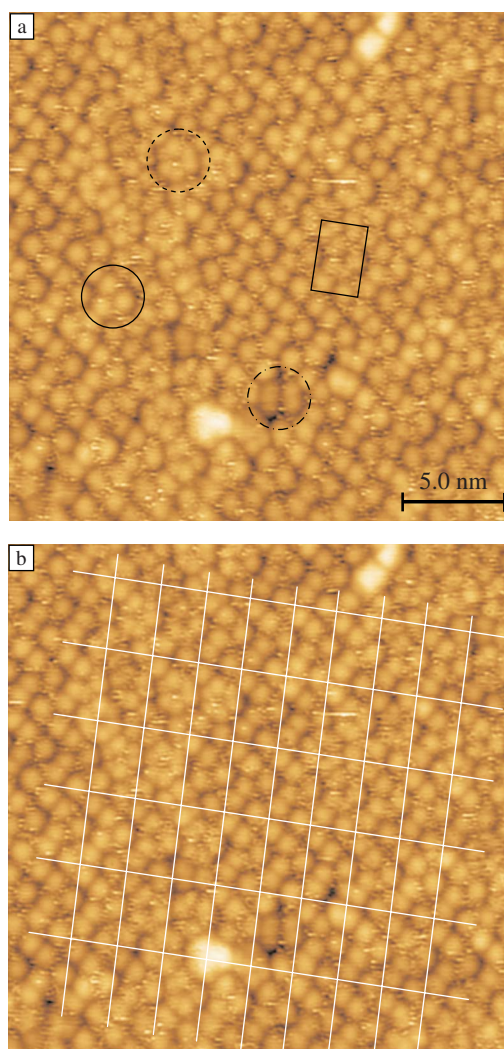


FIG. 5. (Color online) STM images of (a) 4 ML THAP/Au(111) with trigonal molecule (solid circle), hexagonal molecule (dashed circle), and rectangle-pair defect (dash-dotted circle) [unit cell illustrated ( $25.0 \times 25.0 \text{ nm}^2$ ,  $V_{\text{sample}} = -2.5 \text{ V}$ , and  $I = 20 \text{ pA}$ )] and (b) same image with lattice lines drawn to elucidate same molecular ordering as first three monolayers.

#### D. Fourth monolayer

As with the third monolayer of THAP, images of the fourth monolayer were recorded after annealing the sample to desorb excess molecules, in this case at 325 K for 45 min. Again, annealing at such a low temperature is not expected to change the film structure. This is substantiated by the difficulties in acquiring stable images of the fourth monolayer, which would not be the case if one or two monolayers were desorbed. The minimum tunneling current limit (20 pA) of the Omicron system was needed to record topographs with low noise, and even then the tip readily picked up molecules from the surface during scanning, which destabilized the images. The first through third monolayers could be imaged with 60–100 pA, but no images of the fourth monolayer were obtainable with such relatively high currents. The least noisy STM image of the fourth monolayer is shown in Fig. 5(a). It appears as though the image is composed of  $\sim 10 \text{ \AA}$

spheres without any discernible order but with some definite superstructure. In fact, each sphere is one of a triplet of spheres that constitute a single THAP molecule, just as with the third monolayer in Fig. 4(b). Some of the molecules are composed of six smaller features and appear more like hexagons than triangles. Both types of molecule are encircled in Fig. 5(a) in solid and dashed lines. In either case, the overall structure is the familiar hcp herringbone seen in all of the preceding monolayers. For clarity, the image is duplicated in Fig. 5(b) with lattice lines drawn. The unit cell is again rectangular with two molecules per cell and dimensions  $a=21.9 \pm 0.1 \text{ \AA}$ ,  $b=35.8 \pm 0.1 \text{ \AA}$ , and  $\Gamma=88.4 \pm 0.5^\circ$ . As the molecular order and unit cell dimensions of the fourth monolayer agrees with the first three monolayers, and as the first and second monolayers were shown to be commensurate, it can be assumed that the subsequent layers also grow commensurately. This is significant as commensurate growth promotes  $\pi$ -orbital stacking and improves charge carrier hopping.<sup>3</sup>

As noted above, a few molecules consist of six smaller features in a hexagon rather than three spheres in a triangle. From a geometric point of view, these features can be attributed to the outer phenyl groups, but it is unclear why they would be selectively imaged in those molecules instead of the thiophene rings. It may be some underlying defect or molecular deformation which causes such an appearance, or perhaps a local molecule-molecule charge transfer. There is another type of defect in Fig. 5(a) which occurs four times throughout the image. These defects are characterized by a molecular site occupied by a pair of rectangular shaped features, one of which is encircled in the figure by a dash-dotted line. The lattice is not distorted by these defects. By considerations from other STM images, they seem to comprise single THAP molecules somehow tilted and asymmetrically deformed to the current state.

The interesting feature of Fig. 5(a) is the strong localization of molecular density of states. In the third monolayer [Fig. 4(b)], the LDOS appears somewhat localized near the thiophene rings, but there is still a noticeable background of broadened states on each molecule caused by relative proximity to the metal. In the fourth monolayer, the background is no longer observable, as the influence from the metal is less pervasive, and thus the molecules appear only as three spheres arranged in a triangular shape. The LDOS is therefore more strongly concentrated on the thiophene groups in the fourth monolayer than in the third. The spheres, however, are larger than expected from the aforementioned DFT calculations, from which the image in Fig. 4(a) seems a more

likely representative of the HOMO. This can be rationalized as higher bias voltage was used to image the fourth layer as opposed to the third layer. Therefore, a greater number of lower-lying states were accessed, not just those directly on the thiophene groups, which may account for the inflated sphere diameter. Regardless of the sphere radius, images of the third and fourth monolayers illustrate well the gradual attenuation of substrate state broadening effects as molecules farther from the interface are probed.

#### IV. CONCLUSIONS

THAP molecules form well ordered layers on Au(111) up to the fourth monolayer, as determined by STM. The first monolayer orders in an hcp structure with a herringbone pattern defined by alternating rows of molecules with antiparallel orientations. The alternation is presumably caused by steric hindrance between nearest neighbor aromatic cores, and it establishes a rectangular unit cell with two molecules per cell. The second monolayer orders in the same manner, and STM images of partial second layer coverage illustrate that there is commensurate growth between the first two layers. Molecular ordering of the third and fourth monolayers is essentially equivalent to the first two, save for the disordered hcp structure briefly observed in the third monolayer. Growth from the first to fourth monolayers is therefore assumed to be commensurate. This suggests a registry between layers such that one monolayer influences the order and lattice vector directions of the successive layer. Subsequent monolayers are also expected to order in the same fashion. Lastly, STM images from the first to fourth monolayers illustrate the decrease in LDOS broadening effects caused by the Au(111) substrate. Molecules in the first two monolayers appear uniform in contrast, but as thicker layers are probed, the density of states observed by STM more closely resembles the HOMO calculated by DFT for the isolated molecule. Thus, the substrate influences the electronic state distribution for proximal molecules, but farther from the interface the molecular states are less affected and reflect more the isolated case.

#### ACKNOWLEDGMENTS

We acknowledge support from the National Science Foundation (DMR-0705920) and the American Society for Engineering Education NDSEG fellowship. Work at the Georgia Institute of Technology was supported by the National Science Foundation (CHE-0211419 and the STC Program under Agreement No. DMR-0120967), by Lintec Corporation, and by the Office of Naval Research (N00014-04-1-0120).

\*Corresponding author; sieuh@princeton.edu

<sup>1</sup>H. Klauk, M. Halik, U. Zschieschang, G. Schmid, W. Radlik, and W. Weber, *J. Appl. Phys.* **92**, 5259 (2002).

<sup>2</sup>V. Podzorov, S. E. Sysoev, E. Loginova, V. M. Pudalov, and M. E. Gershenson, *Appl. Phys. Lett.* **83**, 3504 (2003).

<sup>3</sup>X. Crispin, J. Cornil, R. Friedlein, K. K. Okudaira, V. Lemaire, A.

Crispin, G. Kestemont, M. Lehmann, M. Fahlman, R. Lazzaroni, Y. Geerts, G. Wendin, N. Ueno, J. L. Brédas, and W. R. Salaneck, *J. Am. Chem. Soc.* **126**, 11889 (2004).

<sup>4</sup>B. R. Kaafarani, T. Kondo, J. Yu, Q. Zhang, D. Dattilo, C. Risko, S. C. Jones, S. Barlow, B. Domercq, F. Amy, A. Kahn, J. L. Brédas, B. Kippelen, and S. R. Marder, *J. Am. Chem. Soc.* **127**,

- 16358 (2005).
- <sup>5</sup>M. Lehmann, G. Kestemont, R. G. Aspe, C. Buess-Herman, M. H. J. Koch, M. G. Debije, J. Piris, M. P. d. Haas, J. M. Warman, M. D. Watson, V. Lemaury, J. Cornil, Y. H. Geerts, R. Gearba, and D. A. Ivanov, *Chem.-Eur. J.* **11**, 3349 (2005).
- <sup>6</sup>S. Barlow, Q. Zhang, Bilal R. Kaafarani, C. Risko, F. Amy, Calvin K. Chan, B. Domercq, Zoya A. Starikova, Mikhail Y. Antipin, Tatiana V. Timofeeva, B. Kippelen, J.-L. Brédas, A. Kahn, and Seth R. Marder, *Chem.-Eur. J.* **13**, 3537 (2007).
- <sup>7</sup>C. K. Chan, F. Amy, Q. Zhang, S. Barlow, S. Marder, and A. Kahn, *Chem. Phys. Lett.* **431**, 67 (2006).
- <sup>8</sup>C. K. Chan, A. Kahn, Q. Zhang, S. Barlow, and S. R. Marder, *J. Appl. Phys.* **102**, 014906 (2007).
- <sup>9</sup>H. E. Katz, J. Johnson, A. J. Lovinger, and W. Li, *J. Am. Chem. Soc.* **122**, 7787 (2000).
- <sup>10</sup>Z. Bao, A. J. Lovinger, and J. Brown, *J. Am. Chem. Soc.* **120**, 207 (1998).
- <sup>11</sup>F. Charra and J. Cousty, *Phys. Rev. Lett.* **80**, 1682 (1998).
- <sup>12</sup>P. Wu, Q. Zeng, S. Xu, C. Wang, S. Yin, and C.-L. Bai, *ChemPhysChem* **2**, 750 (2001).
- <sup>13</sup>M. Palma, G. Pace, O. Roussel, Y. Geerts, and P. Samorì, *Aust. J. Chem.* **59**, 376 (2006).
- <sup>14</sup>L. Askadskaya, C. Boeffel, and J. P. Rabe, *Ber. Bunsenges. Phys. Chem.* **97**, 517 (1993).
- <sup>15</sup>M. Palma, J. Levin, V. Lemaury, A. Liscio, V. Palermo, J. Cornil, Y. Geerts, M. Lehmann, and P. Samorì, *Adv. Mater. (Weinheim, Ger.)* **18**, 3313 (2006).
- <sup>16</sup>S. D. Ha, B. R. Kaafarani, S. Barlow, S. R. Marder, and A. Kahn, *J. Phys. Chem. C* **111**, 10493 (2007).
- <sup>17</sup>J. P. Ibe, J. P. P. Bey, S. L. Brandow, R. A. Brizzolara, N. A. Burnham, D. P. DiLella, K. P. Lee, C. R. K. Marrian, and R. J. Colton, *J. Vac. Sci. Technol. A* **8**, 3570 (1990).
- <sup>18</sup>I. Horcas, R. Fernández, J. M. Gómez-Rodríguez, J. Colchero, J. Gómez-Herrero, and A. M. Baro, *Rev. Sci. Instrum.* **78**, 013705 (2007).
- <sup>19</sup>N. H. Tinh, H. Gasparoux, and C. Destrade, *Mol. Cryst. Liq. Cryst.* **68**, 101 (1981).
- <sup>20</sup>J. A. Kubby and J. J. Boland, *Surf. Sci. Rep.* **26**, 61 (1996).
- <sup>21</sup>J. V. Barth, H. Brune, G. Ertl, and R. J. Behm, *Phys. Rev. B* **42**, 9307 (1990).
- <sup>22</sup>S. Narasimhan and D. Vanderbilt, *Phys. Rev. Lett.* **69**, 1564 (1992).
- <sup>23</sup>N. Nicoara, E. Roman, J. M. Gomez-Rodríguez, J. A. Martin-Gago, and J. Mendez, *Org. Electron.* **7**, 287 (2006).
- <sup>24</sup>F. Sellam, T. Schmitz-Hubsch, M. Toerker, S. Mannsfeld, H. Proehl, T. Fritz, K. Leo, C. Simpson, and K. Mullen, *Surf. Sci.* **478**, 113 (2001).
- <sup>25</sup>C. R. Safinya, N. A. Clark, K. S. Liang, W. A. Varady, and L. Y. Chiang, *Mol. Cryst. Liq. Cryst.* **123**, 205 (1985).
- <sup>26</sup>R. Strohmaier, C. Ludwig, J. Petersen, B. Gompf, and W. Eisenmenger, *J. Vac. Sci. Technol. B* **14**, 1079 (1996).
- <sup>27</sup>H. Vazquez, F. Flores, R. Oszwaldowski, J. Ortega, R. Perez, and A. Kahn, *Appl. Surf. Sci.* **234**, 107 (2004).